Solar Physics (2006) 238: 167–186
DOI: 10.1007/s11207-006-0185-3

A NEW PREDICTION METHOD FOR THE ARRIVAL TIME OF INTERPLANETARY SHOCKS

XUESHANG FENG
SIGMA Weather Group, State Key Laboratory for Space Weather, Center for Space Science and Applied Research, Beijing 100080, China

and

XINHUA ZHAO
SIGMA Weather Group, State Key Laboratory for Space Weather, Center for Space Science and Applied Research, Beijing 100080, China; Graduate University of the Chinese Academy of Sciences, Beijing 100049, China

(Received 26 March 2006; accepted 31 July 2006; Published online 9 October 2006)

Abstract. Solar transient activities such as solar flares, disappearing filaments, and coronal mass ejections (CMEs) are solar manifestations of interplanetary (IP) disturbances. Forecasting the arrival time at the near Earth space of the associated interplanetary shocks following these solar disturbances is an important aspect in space weather forecasting because the shock arrival usually marks the geomagnetic storm sudden commencement (SSC) when the IMF *Bz* component is appropriately southward and/or the solar wind dynamic pressure behind the shock is sufficiently large. Combining the analytical study for the propagation of the blast wave from a point source in a moving, steady-state, medium with variable density (Wei, 1982; Wei and Dryer, 1991) with the energy estimation method in the ISPM model (Smith and Dryer, 1990, 1995), we present a new shock propagation model (called SPM below) for predicting the arrival time of interplanetary shocks at Earth. The duration of the X-ray flare, the initial shock speed and the total energy of the transient event are used for predicting the arrival of the associated shocks in our model. Especially, the background speed, i.e., the convection effect of the solar wind is considered in this model. Applying this model to 165 solar events during the periods of January 1979 to October 1989 and February 1997 to August 2002, we found that our model could be practically equivalent to the prevalent models of STOA, ISPM and HAFv.2 in forecasting the shock arrival time. The absolute error in the transit time in our model is not larger than those of the other three models for the same sample events. Also, the prediction test shows that the relative error of our model is $\leq$10% for 27.88% of all events, $\leq$30% for 71.52%, and $\leq$50% for 85.46%, which is comparable to the relative errors of the other models. These results might demonstrate a potential capability of our model in terms of real-time forecasting.

1. Introduction

It is well known that various kinds of solar transient activities such as solar flares, disappearing filaments, and coronal mass ejections (CMEs) are responsible for strong interplanetary (IP) disturbances and corresponding non-recurrent geomagnetic disturbances. The IP shocks in the solar wind plasma associated with CMEs, solar flares, and stream–stream interactions herald the initiation of geomagnetic storms if sufficiently long and sufficiently large-magnitude southward components of the interplanetary magnetic field exist following the shocks (Dryer, 1994). Therefore, predicting the arrival times of these IP shocks at the near Earth space with enough lead time has become a crucial aspect in space weather forecasting. Several models aimed at forecasting the arrival time of IP shocks at 1 AU have been developed, to list a few, such as the shock time of arrival model (STOA), the interplanetary shock propagation model (ISPM) and the modified Hakamada–Akasofu–Fry/version-2 (HAFv.2) model. These three models have been widely used in real-time prediction of the arrival time and the comparison between the results of our new method with those obtained from them will be presented in this paper. Thus, brief description for the models of STOA, ISMP, and HAFv.2 is given later.

The STOA model is based on similarity theory of blast waves, modified by the piston-driven concept, which emanate from point explosions (Dryer, 1974; Dryer and Smart, 1984; Smart *et al.*, 1984, 1986; Smart and Shea, 1985; Lewis and Dryer, 1987). In this model, the initial explosion (flare) drives a shock and the shock is assumed to have a constant speed (V_s) for a specified length of time τ that is estimated using the X-ray duration of the flare. Then the shock decelerates to a blast wave as it expands outwards with $V_s \sim R^{-1/2}$ (where R is the heliocentric radial distance). The magnitude of the total energy released determines the solid angle of quasi-spherical shock propagation as well as how far a particular shock will propagate as it "rides over" a uniform background solar wind. The fastest part of the shock is believed to be nearly coincident with the radius vector from the center of the Sun through the flare site. The shock speed directly above the flare is calculated from the type II radio frequency drift rate based on an assumed coronal density model. STOA uses a cosine function to account for the longitudinal dependence of the shock geometry in the ecliptic plane. The shock speed is supposed to decrease from maximum in the direction of the flare via this cosine function to provide a nonspherical shape in longitude. This spatially-dependent shock speed is taken to be constant during the piston-driving phase, and the longitudinal cosine function is maintained during the decelerating blast wave phase. STOA considers a radially variable background solar wind speed through which the shock propagates, and this background solar wind speed is estimated from the solar wind velocity V_{SW} measured at L1 at the time of the flare. Required observational data of STOA are as follows: solar flare longitude; start time of the metric type II radio burst; the initial shock speed; the duration of the X-ray flare; and V_{SW}. Beside the arrival time of the shock at any point in the ecliptic plane (referring to Earth in this paper), STOA can provide the shock's Alfvén Mach number Ma as an indicator of the expected shock strength.

The ISPM is based on a 2.5D MHD parametric study of numerically simulated shocks that shows the organizing parameter to be the net energy input to the solar wind (Smith and Dryer, 1990, 1995). If the net energy injected into the solar wind by a solar event and the source's longitude are known, then the transit time and strength of the shocks at 1 AU can be computed from algebraic equations in this model. However, the energy released by a solar event cannot be measured directly. A method is given in ISPM to estimate the net input energy from proxy input data. The same observational data as STOA used are employed in ISPM except for the L1 background solar wind speed V_{SW}. Instead, ISPM selects a fixed radial solar wind profile with $V_{SW} = 340$ km s^{-1} at 1 AU. ISPM also provides the shock strength index (SSI), computed from the logarithm (base 10) of the normalized dynamic pressure jump, as an indicator of confidence of the prediction.

The HAFv.2 model is a "modified kinematic" solar wind model that calculates the solar wind speed, density, magnetic field, and dynamic pressure as a function of time and location (Fry *et al.*, 2001, 2003, 2004). This model has significant advantages over other shock propagation models because it gives a global picture of multiple and interacting shocks that propagate into nonuniform, stream–stream interacting solar wind flows. Specifically, the radial magnetic field at the source surface $R = 2.5R_s$, and the solar wind speed obtained from the prediction method by Arge and Pizzo (2000), are used as an input to HAFv.2. Disturbance energy is made manifest by enhanced solar wind speed at the source surface. HAFv.2 generally uses the same observational inputs as STOA and ISPM but differs from them in considering the background solar wind. That is, realistic inner boundary conditions determine the background solar wind flow and IMF topology in this model. And these data are derived from synoptic solar source surface maps and calculations of the magnetic flux divergence. As for output, HAFv.2 predicts the solar wind speed, density, dynamic pressure, and IMF vector at any point in the heliosphere with time. A Shock Searching Index (SSI_H) is computed at L1, and a predicted shock arrival time is given when this index exceeds an empirical threshold value.

The performances of the above three models have been tested and the comparative study revealed that the performances of these three models were practically identical in forecasting the shock arrival time (McKenna-Lawlor *et al.*, 2002; Fry *et al.*, 2003; Cho *et al.*, 2003; McKenna-Lawlor *et al.*, 2006).

It may be noticed that other methods have also been developed to predict the arrival time of a solar disturbance at Earth. Gopalswamy *et al.* (2000, 2001) gave an empirical model to predict the arrival time of a CME based on its speed observed with the coronagraph. This model was extended to predict the IP shock arrival at Earth by using the piston–shock relationship between the CME speed and the speed of the shock ahead of the CME (Gopalswamy *et al.*, 2005). By combining the observations of solar activity, interplanetary scintillation (IPS), and geomagnetic disturbance observations together with the dynamics of solar wind storm propagation (S) and fuzzy mathematics (F), Wei and his coworkers (Wei and Cai, 1990; Wei, Xu, and Feng, 2002; Wei, Cai, and Feng, 2003; Wei *et al.*, 2005) gave a new "ISF" prediction method for geomagnetic disturbances caused by solar wind storms traveling to Earth. Manoharan *et al.* (2004) provided an empirical method to predict the IP shock transit time to 1 AU based on the CME initial speed. Schwenn *et al.* (2005) presented a prediction function of the shock's arrival time at Earth by fitting the transit time with the lateral expansion speed of the CME. Anyway, the prediction of the arrival time of solar disturbances is an interesting topic in space weather. Besides the methods given earlier, there are still many other methods left unmentioned. Here we are not aiming at exhausting all the methods of this aspect.

The paper is organized as follows. In Section 2, the analytical solutions on the propagation of the blast wave from a point source in a moving medium with variable density (Wei, 1982; Wei and Dryer, 1991) are presented. The method to estimate the net energy of a solar event is discussed. Then a new shock propagation model (SPM) is put forward, and a set of 165 solar events as training data are used to evaluate and improve the performance of the SPM model. In Section 3, the comparisons of prediction results between our model and the models of STOA, ISPM, and HAFv.2 are presented. Conclusions are given in Section 4.

2. Shock Propagation Model

2.1. Analytical solutions of blast waves

This section recalls Wei's nonsimilarity theory on analytical solutions to the propagation of the blast wave. Wei and his coworkers (Wei, 1982; Wei, Yang, and Zhang, 1983) studied theoretically the propagation of the blast wave from a point source in a moving, steady-state, medium with variable density, and got some analytical solutions. In order for our paper to be self-contained, we will give some details of the derivation of their analytical solution. They started from the basic equations of ideal fluid dynamics under a spherically symmetric hypothesis:

$$
\begin{aligned}
&\frac{\partial \rho}{\partial t} + u\frac{\partial \rho}{\partial r} + \rho\left(\frac{\partial u}{\partial r} + \frac{2u}{r}\right) = 0,\\
&\rho\left(\frac{\partial u}{\partial t} + u\frac{\partial u}{\partial r}\right) + \frac{\partial p}{\partial r} = 0,\\
&\frac{\partial p}{\partial t} + u\frac{\partial p}{\partial r} + \gamma p\left(\frac{\partial u}{\partial r} + \frac{2u}{r}\right) = 0.
\end{aligned}
$$

Dimensionless variables, such as e.g. $x = r/R$, $y = u_0/V_s$, $f = u/V_s$, are introduced, and the previous equations are rewritten into dimensionless forms. Here $V_s = dR/dt$ is the shock speed, R is the radial distance (in AU) to which the shock has propagated, and u_0 is the background solar wind speed. Wei (1982) and Wei, Yang, and Zhang (1983) solved the equations after modifying Sedov's classical similarity theory for the blast waves to include a steady-state, background solar wind velocity u_0. In this spherically symmetric model, the energy released by the point blast into the background solar wind is supposed to be:

$$E_s = \int_0^R \left[\left(\frac{1}{2}\rho u^2 + \frac{p}{\gamma - 1} \right) - \left(\frac{1}{2}\rho_0 u_0^2 + \frac{p_0}{\gamma - 1} \right) \right] r^2 \mathrm{d}r = \text{constant}. \tag{1}$$

The dimensionless variables such as $f = u/V_s$, $h = \rho/\rho_0 = (\rho/A)r^2$, $g = p/(\rho_0 V_s^2)$ are introduced; Here A (=300 kg m^{-1}) is a constant of proportionality in the inverse density relationship $\rho = A/R^2$. Then Equation (1) can be written in its dimensionless form:

$$E_s = \frac{Au_0^2}{y^2} \int_0^1 \left(\frac{1}{2}hf^2 + \frac{g}{\gamma - 1} \right) \mathrm{d}x - \frac{Au_0^2 R}{2}. \tag{2}$$

Let us define $E_0 = E_s/Au_0^2$ and $J = \int_0^1 (1/2hf^2 + g/\gamma - 1)\mathrm{d}x$, then this equation can be abbreviated as:

$$J = \left(\frac{E_0}{R} + \frac{1}{2} \right) y^2. \tag{3}$$

E_0 represents the dimensionless form of the total energy E_s. Differentiating this equation with respect to y, then:

$$\frac{E_0}{R} y^2 = \lambda \left(J - \frac{1}{2} y \frac{\mathrm{d}J}{\mathrm{d}y} \right) \tag{4}$$

with $\lambda = 2(R/y)(\mathrm{d}y/\mathrm{d}R)$. If J is expanded as $J = J_0(1 + \sigma_1 y + \sigma_2 y^2 + \cdots)$, then Equation (3) combined with Equation (4) can give

$$\sigma_1 = 2\lambda_1 + \frac{\sigma_1}{2}, \quad \sigma_1 = 4\lambda_1. \tag{5}$$

Following Wei (1982), the first order approximation of $J_0(1+\sigma_1 y) = J_0(1+4\lambda_1 y)$ is adopted to represent the total energy J because of the difficulty in solving higher order equations. Therefore,

$$\left(\frac{E_0}{R} + \frac{1}{2} \right) y^2 \doteq J_0(1 + 4\lambda_1 y). \tag{6}$$

The dimensionless variable $y = u_0/V_s$ is solved from Equation (6) to give:

$$V_s = \frac{\mathrm{d}R}{\mathrm{d}t} = \left[-2\lambda_1 + \sqrt{(2\lambda_1)^2 + \frac{E_0}{J_0 R} + \frac{1}{2J_0}} \right] u_0. \tag{7}$$

Here $J_0 = 3/8$, $\lambda_1 = -0.1808$, are obtained in solving the basic equations of ideal fluid (Wei, 1982; Wei, Yang, and Zhang, 1983). The details about the process of solving these equations can be seen in these related papers.

The integral of Equation (7) gives the transit time (TT) of the shock to reach a position R:

$$\mathrm{TT} = \int \frac{\mathrm{d}R}{V_s} = \int \frac{\mathrm{d}R}{-2u_0\lambda_1 + u_0\sqrt{(2\lambda_1)^2 + \frac{E_0}{J_0 R} + \frac{1}{2J_0}}}. \tag{8}$$

That is,

$$\begin{aligned}
\mathrm{TT} = \frac{J_0}{u_0}\Bigg\{ & 4\lambda_1[R + 2E_0 - 2E_0\ln(R + 2E_0)] + 2\sqrt{X} - \frac{\left(16\lambda_1^2 + \frac{1}{J_0}\right)E_0}{\sqrt{4\lambda_1^2 + \frac{1}{2J_0}}} \\
& \times \ln\left[\sqrt{X} + (R + 2E_0)\sqrt{4\lambda_1^2 + \frac{1}{2J_0}} - \frac{\left(16\lambda_1^2 + \frac{1}{J_0}\right)E_0}{2\sqrt{4\lambda_1^2 + \frac{1}{2J_0}}}\right] \\
& - 8\lambda_1 E_0 \times \ln\left[\frac{\sqrt{X} + 4\lambda_1 E_0}{(R + 2E_0)} - \frac{\left(16\lambda_1^2 + \frac{1}{J_0}\right)}{8\lambda_1}\right]\Bigg\} + \mathrm{TT}_0. \qquad (9)
\end{aligned}$$

Here

$$\sqrt{X} = \sqrt{\frac{E_0}{J_0}R + \left(4\lambda_1^2 + \frac{1}{2J_0}\right)R^2},$$

and TT_0 is determined by the restriction of $R = 0$ when $\mathrm{TT} = 0$. Following Wei (1982), in order to demonstrate the contribution of the energy and background solar wind speed to the shock's transit time, we show the dependence of the transit time to 1 AU predicted by Equation (9) on the energy and solar wind speed in Figure 1. It can be seen from Figure 1(a) that the transit time decreases with the increase of the energy. Similarly, Figure 1(b) reveals that the transit time decreases with the increase of the solar wind speed for a given total energy, especially for low energy cases. This demonstrates that the energy and solar wind speed are two important factors contributing to the shock's transit time to 1 AU. The transit time depends on the energy released in a specific solar event as well as on the background speed. Wei (1982) used this solution to analyze the shock's deceleration in the interplanetary space and pointed out that the deceleration process is nonuniform. The shock slows down only slightly at large heliocentric radial distances due to the

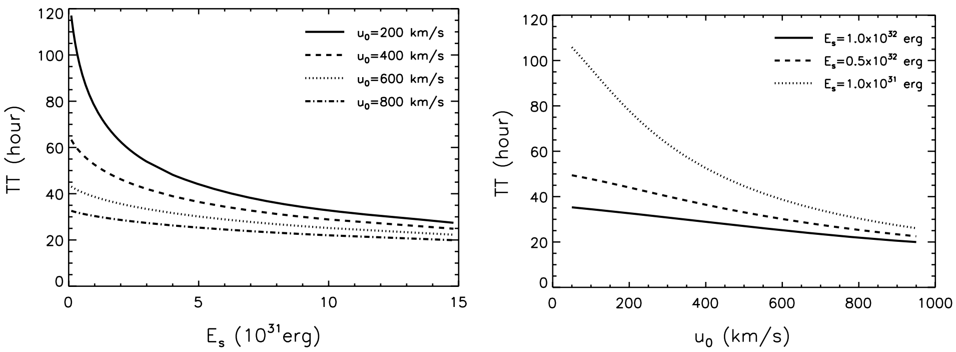

(a) (b)

Figure 1. The shock transit time versus the total energy (a) and the background solar wind speed (b).

convective effect of the solar wind, so that the shock could propagate far beyond 10–20 AU without any significant decay during this passage. This phenomenon can be confirmed by the observation that the shock velocity can reach 900 km s^{-1} at 7–16 AU as detected by Pioneer 10 and 11 following the big flare (3B, N22E38) on April 28, 1978 (Wei, 1982).

Wei and Dryer (1991) used Equation (9) together with the IPS observations to study the propagation characteristics of flare-associated interplanetary shocks. Also based on interplanetary scintillation (I) together with the dynamics of solar wind storm propagation (S) and fuzzy mathematics (F), the so-called "ISF" prediction method was proposed (Wei and Cai, 1990; Wei, Xu, and Feng, 2002; Wei, Cai, and Feng, 2003; Wei *et al.*, 2005) to predict the start time of geomagnetic disturbances caused by solar wind storms traveling to Earth. In the ISF method, IPS observations are used to provide parameters (R_s, T_s, u_0). Here, R_s stands for the heliocentric radial distance of the shock when it transits across the line-of-sight to fixed IPS radio sources, T_s stands for the time of the shock's arrival at R_s, and u_0 is the solar wind speed. Hence, the energy can be calculated from Equation (9) given (R_s, T_s, u_0). Then, this energy together with the solar wind speed u_0 are used as inputs to Equation (9) for predicting the shock's arrival time at Earth. In what follows, we try to directly estimate the energy released by a solar transient event based on observations at the Sun for the sake of real-time forecasting.

2.2. Estimation of the Energy

The total energy of a solar event is naturally an important parameter for the propagation of interplanetary disturbances. Smith and Dryer (1990) performed a 2.5D MHD simulations on the interplanetary shock propagation and found that the net input energy determines the forward shock properties such as the transit time, strength, and angular extent at 1 AU. However, the total energy of a solar event is not readily available from direct observations. Some forms of proxy need to be adopted. The ISPM model (Smith and Dryer, 1990, 1995) assumes that the total energy of the event is proportional to V_s^3 (kinetic energy flux), and the dependence of the event energy on the longitudinal width ω and the duration τ of the initial pulse is also assumed to be linear. Based on these assumptions, Smith and Dryer (1990, 1995) established an empirical expression for the total energy of the event as by

$$E_s = C V_s^3\, \omega(\tau + D), \tag{10}$$

here C and D are assumed to be constant with their values being $0.283 \times 10^{20}(\mathrm{erg\,m^{-3}\,s^{-2}\,deg^{-1}})$ and 0.52 (hour) respectively; Also, an average of angular width $\omega_A = 60^\circ$ is used in ISPM, and the duration time (τ) longer than 2 hours is automatically truncated to 2 hours. Using the net energy from Equation (10) as input, the ISPM model successfully provides us a method of forecasting the shock arrival time. Therefore, it can be believed that Equation (10) is a good candidate for the net energy estimation for a specific solar event, which will be employed in our following discussion.

2.3. Model description and its tentative training

In this section, we first present our tentative results on the prediction of the arrival time based on Equations (9) and (10), and then provide a modification according to our test results and the observation. For training purposes, we have collected 165 solar flare interplanetary shock events that arrived at Earth during the periods of January 1979 to October 1989 (28 events) and February 1997 to August 2002 (137 events) from published papers (Smith and Dryer, 1995; Fry *et al.*, 2003; McKenna-Lawlor *et al.*, 2006). In these papers, the STOA, ISPM, and HAFv.2 models have been used, respectively, to predict the arrival times of these shock events. The events without any geo-effects or shock arrival at near Earth space or those for which there exists no unique correlation between the solar event and the corresponding shock at 1 AU are excluded from our sample.

Now we turn to our tentative prediction for the arrival time. First, the initial shock speed and duration of the event are inserted into Equation (10) to estimate the energy associated with the event (ω taken as 60°). Then the estimated energy together with the background solar wind speed are used to predict the transit time via Equation (9) for these 165 events. Let us look at the prediction error defined by $\Delta\mathrm{TT} = \mathrm{TT}_{\mathrm{obs}} - \mathrm{TT}_{\mathrm{pred}}$, where $\mathrm{TT}_{\mathrm{obs}}$ and $\mathrm{TT}_{\mathrm{pred}}$ stand for the observed and predicted transit times. It is well known that the energy released by a solar event plays an important role in the shock's arrival. This motivates us to consider the relationship between the prediction error and the energy. Figure 2 gives the prediction error

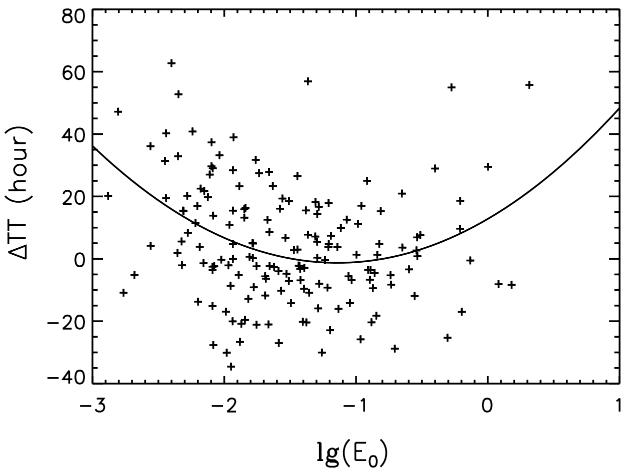

Figure 2. The error in the predicted transit time (ΔTT given by Equation (9)) plotted versus $\lg(E_0)$. The solid curve denotes a quadratic fitting.

plotted against the dimensionless energy E_0. As expected, this figure demonstrates that the error has notable correlation with E_0. The solid curve denotes the binomial fitting $\Delta\mathrm{TT} = 12.789 + 24.692\,\lg(E_0) + 10.8314[\lg(E_0)]^2$, which can well depict the correlation as seen. This correlation between ΔTT and E_0 implies that it might be inappropriate to use Equation (9) alone. In fact, the origin of this defect may be twofold. On one hand, the magnetic field is neglected in our formulation. On the other hand, the IP shocks are treated as the blast wave in this analytic solution, which is not the general case after all. Especially, in the derivation of the analytic solution, only the first-order terms of energy were considered, and higher order terms were neglected as seen in Section 2.1. These might partially explain why ΔTT given by Equation (9) are correlated with E_0. As for other parameters such as the shock speed V_s and background solar wind speed u_0, no evident correlation between them and ΔTT is found in the test. Taking account of all these arguments, we are now in a position to state that our new shock propagation model (SPM) for predicting the transit time is as follows:

$$\begin{aligned}\mathrm{TT} = \frac{J_0}{u_0}\Bigg\{ & 4\lambda_1[R + 2E_0 - 2E_0\ln(R + 2E_0)] + 2\sqrt{X} - \frac{\left(16\lambda_1^2 + \frac{1}{J_0}\right)E_0}{\sqrt{4\lambda_1^2 + \frac{1}{2J_0}}} \\ & \times\ln\left[\sqrt{X} + (R + 2E_0)\sqrt{4\lambda_1^2 + \frac{1}{2J_0}} - \frac{\left(16\lambda_1^2 + \frac{1}{J_0}\right)E_0}{2\sqrt{4\lambda_1^2 + \frac{1}{2J_0}}}\right] - 8\lambda_1 E_0 \\ & \times\ln\left[\frac{\sqrt{X} + 4\lambda_1 E_0}{(R + 2E_0)} - \frac{\left(16\lambda_1^2 + \frac{1}{J_0}\right)}{8\lambda_1}\right]\Bigg\} + \mathrm{TT}_0 + \Delta\mathrm{TT}(E_0) \end{aligned} \tag{11}$$

where $\triangle\mathrm{TT}(E_0) = 12.789 + 24.692\,\lg(E_0) + 10.8314[\lg(E_0)]^2$, and E_0 is determined by Equation (10).

In the following, the SPM model will be used to predict the transit time for these 165 events, and comparisons of our results will be made with those of the other three prevalent models of STOA, ISPM, and HAFv.2.

3. Prediction Results and Comparisons

By applying the SPM model (Equations (10)–(11)) to the data set of 165 events, we compute the difference between predicted and observed transit time, i.e., $\Delta\mathrm{TT}_{\mathrm{spm}} = \mathrm{TT}_{\mathrm{spm}} - \mathrm{TT}_{\mathrm{obs}}$. Here $\mathrm{TT}_{\mathrm{spm}}$ denotes the predicted transit time by the SPM model, and $\Delta\mathrm{TT}_{\mathrm{spm}}$ denotes its prediction error. The mean absolute error of this model is 14.32 hours for the total 165 events. The STOA model only gives the transit time prediction for 154 events among the total 165 events. While for the remaining events, STOA forecasts that the shock would not be able to arrive at Earth. The mean absolute error of the STOA model is 14.24 hours for these 154

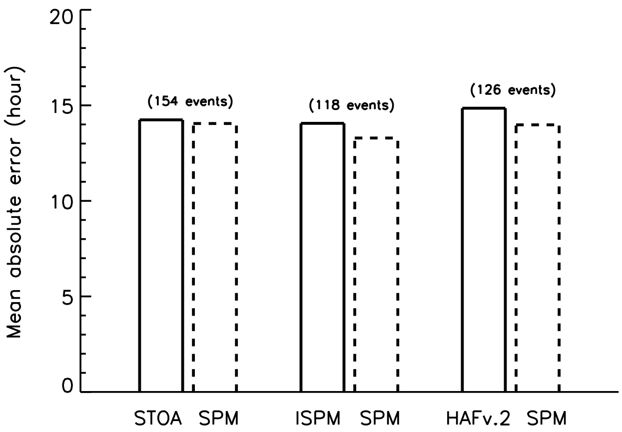

Figure 3. Comparisons of the mean absolute errors of STOA, ISPM and, HAFv.2 models against the SPM.

events. In order to compare with the STOA model, we compute the mean absolute error of our SPM model for the same 154 events on which STOA can predict the transit time, and found that the mean error is 14.05 hours. Similarly, the ISPM model gives prediction for 118 events among the total 165 events with the mean absolute error of 14.06 hours. The mean error of our SPM model for the same 118 events is 13.29 hours. The HAFv.2 model predicts the shock transit time for 126 events among 165 events with the mean absolute error of 14.85 hours, and the mean error of our SPM mode is 13.98 hours for the same 126 events. The comparisons of the mean absolute error between the SPM model and the other three models are displayed in Figure 3. The mean absolute errors of these models are nearly identical, which shows similar capability of forecasting the IP shock arrival time between these models.

Figure 4 gives the histograms of errors in the predicted transit time (ΔTT) for the STOA, ISPM, HAFv.2, and our SPM models. These histograms show Gaussian distributions with a peak around zero. This property of approximate normal distribution demonstrates that the propagations of the IP shocks are mainly accounted for by these models and may be influenced additionally by other factors. However, other error sources, such as coronal density distribution, complex heliospheric environments, and solar wind inhomogeneities (Moon *et al.*, 2002; Cho *et al.*, 2003), can also influence the propagation and arrival of IP shocks and may lead to complicated distributions of ΔTT. And these error sources can explain, at least partly, the fact that the mean absolute errors of these four models are all above 12 hours.

As for the relative error of predictions, i.e.,

$$\sigma = \frac{|\mathrm{TT}_{\mathrm{obs}} - \mathrm{TT}_{\mathrm{pred}}|}{\mathrm{TT}_{\mathrm{obs}}},$$

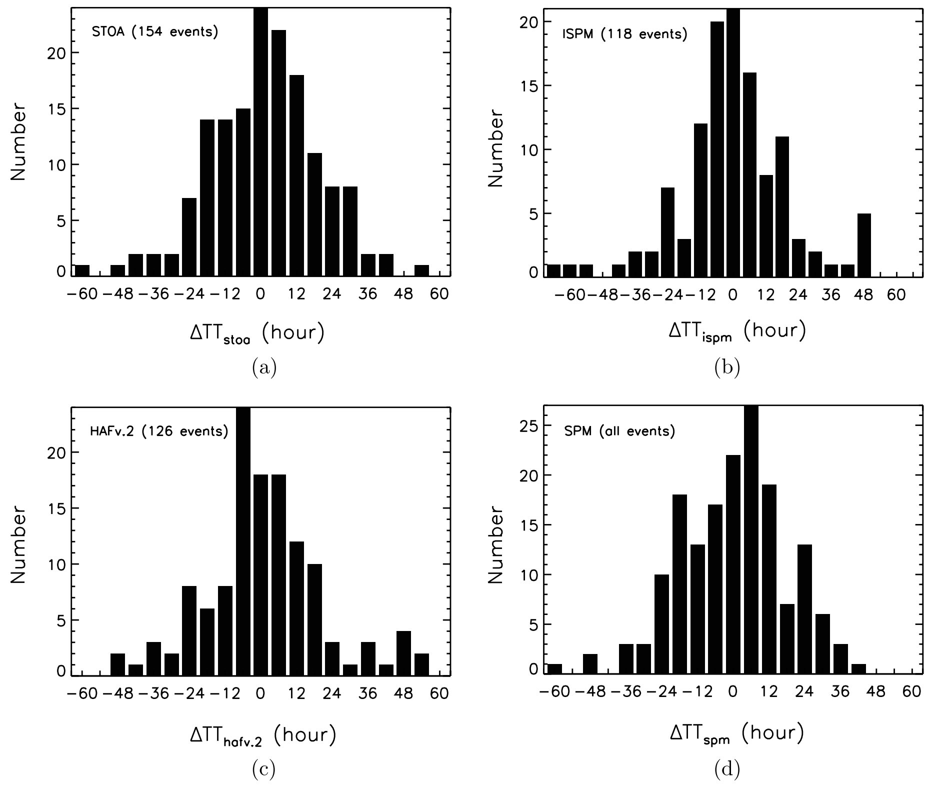

Figure 4. Histograms showing the transit time error ($\triangle$TT) between predicted and observed values for the ensemble of models. The transit time error is based on the STOA, ISPM, HAFv.2, and SPM models.

the prediction test for σ shows that the relative error of our SPM model is $\leq$10% for 27.88% of the total 165 events, $\leq$30% for 71.52%, and $\leq$50% for 85.46%. Table I shows the event percentage at different relative error range for the models of STOA, ISPM, and HAFv.2. The event percentage at the same relative error range for our SPM model is also given for the same events predicted by these three models. We can see from Table I that the performances of the four models in terms of relative errors are nearly identical as well.

For further comparing the prediction results of these models, we express the observed and predicted transit times of the shock in terms of the initial shock speed using a quadratic function (Figure 5). The solid curve denotes the observed transit time (TT_{obs}). The shock transit time to 1 AU decreases as the initial shock speed increases, as expected. The other curves denote the predicted transit time by the four models. In this figure, the fitted prediction curves show a trend similar to the fitted observation curve, they all intersect at $V_s \approx 900$ km s^{-1}. This indicates that these four models have captured the dependence of transit time on the shock

TABLE I

Comparisons of the relative errors (σ) in the STOA, ISPM, HAFv.2, and SPM models.

	Event percentage		
	$\sigma \leq 10\%$	$\sigma \leq 30\%$	$\sigma \leq 50\%$
SPM (all events)	27.88	71.52	85.46
STOA (154 events)	25.97	70.78	85.07
SPM (same events)[a]	27.92	71.43	85.71
ISPM (118 events)	28.81	73.73	86.44
SPM (same events)[b]	32.20	71.19	85.59
HAFv.2 (126 events)	28.57	68.25	88.89
SPM (same events)[c]	27.78	72.22	85.71

[a]The same 154 events predicted by STOA.
[b]The same 118 events predicted by ISPM.
[c]The same 126 events predicted by HAFv.2.

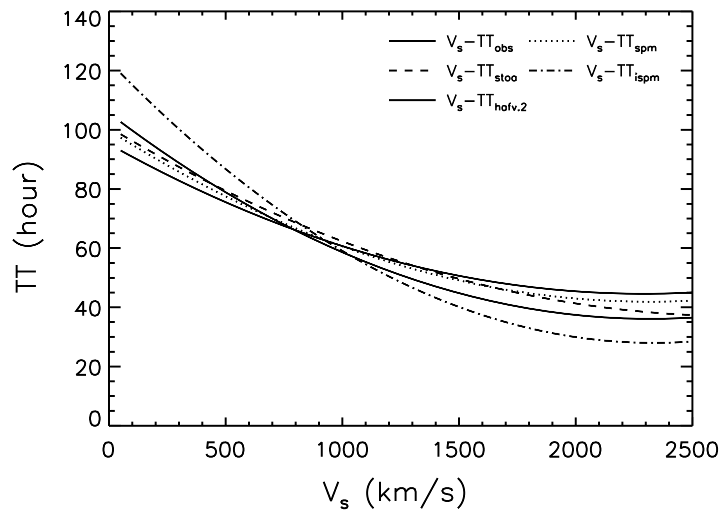

Figure 5. The shock transit times fitted by quadratic functions of the shock initial speed. The *solid curve* corresponds to the observed transit time, while the *other curves* represent the predictions by the STOA, ISPM, HAFv.2, and SPM models.

speed very well, and therefore the basic assumptions in these models have been vindicated. Particularly, the SPM prediction curve (dotted line) is closer to the observation curve (solid line) than the other three curves in both low-speed and high-speed ranges. This further demonstrates that our model is comparable to, or even a little better than, the other three prevalent models in forecasting the shock arrival time.

4. Conclusions

We have introduced a new model (SPM) for predicting the arrival time of IP shocks at Earth based on the analytic solutions about the propagation of blast waves in a moving medium with variable density. By a simple analytic solution, the SPM model uses the duration of the X-ray event, the initial shock speed, the background solar wind speed and the energy released in the solar event as input to predict the arrival time. In this model, the duration of the X-ray event and the initial shock speed are used to estimate the energy (like that in the ISPM model) of the solar event. Applying the SPM model to 165 solar events during the periods of January 1979 to October 1989 and February 1997 to August 2002, we found that the performance of our model is as good as those of the prevalent models of STOA, ISPM, and HAFv.2 in predicting the shock arrival time. Meanwhile, our SPM model expressed in analytic form can promptly provide us the arrival time if the duration of the X-ray event, the initial shock speed, and the background solar wind speed for a specific solar event are known, which are usually available by present solar observations. This demonstrates the feasibility of our model as one of the prediction methods in real-time space weather forecasting.

However, like other similar arrival time prediction models our SPM model has also its own shortcomings. On the one hand, the SPM does not take into account of other factors, such as coronal density inhomogeneities, coronal holes, helmet streamers, structure of the heliospheric current sheet (HCS), interaction of disturbances, fluctuation in solar-wind speed, and their combinations, which would contribute to the shock's transit time to 1 AU (Heinemann, 2002; Moon *et al.*, 2002). On the other hand, not all solar transient phenomena can arrive at Earth because of the attenuation during their propagation in the interplanetary space and/or their propagation direction far away from the Sun–Earth line. In the other models like STOA, ISPM, and HAFv.2, some useful index (such as *M*a and SSI), used as an indicator of confidence in the prediction, are adopted to evaluate whether a shock would arrive at Earth. These considerations should be included in a future study.

Acknowledgements

This work is jointly supported by the National Natural Science Foundation of China (40536029, 40336053, 40374056, and 40523006), 973 project under grant 2006CB806304 and the International Collaboration Research Team Program of the Chinese Academy of Sciences.

Appendix

The following tables summarize the event parameters and arrival times predicted by STOA, ISPM, HAFv.2, and our SPM models.

TABLE II

Input parameters of the 28 events during the period January 1979 to October 1989. These events are taken from Smith and Dryer (1995).

Event number	Begin date	Begin time (UT)	Source location	V_s (km s^{-1})	τ (hour)	V_{SW} (km s^{-1})	Flare classification X-ray/optical
1	790103	2148	S12W02	1400	0.10	412	M1.0/?B
2	790216	0149	N16E59	1222	0.90	390	X2.0/3B
3	790502	1700	N20W55	1100	0.45	360	X1.0/2B
4	790704	0219	N07E44	2500	1.93	309	C7.0/2N
5	790704	1920	N21E36	1444	1.80	308	M1.0/1B
6	791106	0516	N19E11	1350	1.10	373	X1.0/1N
7	791108	0118	N31E73	1380	0.58	420	M5.0/1B
8	791219	2212	S15E36	1500	0.42	370	X1.0/2B
9	800409	2237	S10W90	1500	1.37	424	C7.0/2B
10	800521	2057	S14W15	1068	0.77	400	X1.0/3B
11	800603	2133	S14E65	1600	0.55	301	M7.0/2B
12	800822	0533	N09E58	1300	0.12	385	M1.0/1B
13	810215	1901	N15W71	795	0.35	377	M1.0/1B
14	810226	1953	S14E49	1200	0.25	338	X4.0/3B
15	810404	0508	S44W88	1000	0.03	400	X1.0/2B
16	810410	1110	N11E53	1807	0.62	419	X1.0/1B
17	810410	1649	N08W36	3553	0.73	419	X2.0/3B
18	810424	1355	N18W50	1970	1.42	500	X6.0/2B
19	810513	0405	N11E55	1500	2.00	500	X2.0/3B
20	810516	0824	N14E14	1750	2.00	450	X1.0/3B
21	810828	0347	N10W44	1678	0.12	337	M6.0/1B
22	820603	1144	S09E72	1000	0.38	652	X8.0/2B
23	820606	1634	S09E25	1250	1.25	650	X9.0/3B
24	820615	1512	S22E66	2750	2.00	310	X1.0/2B
25	820618	2146	N19W11	1000	0.40	448	M1.0/1B
26	820619	1958	N14W24	600	0.25	331	M2.0/2B
27	820722	1720	N16W89	2250	2.00	420	M4.0/1N
28	891019	1249	S27E10	2200	2.00	400	X13.0/4B

The events without corresponding geo-effect or shock arrival are not included here.
Begin time: year month day (YYMMDD), and time in UT of the start of the metric type II radio burst.
Source location: location of the associated optical flare.
V_s: velocity of the shock in the coronal, estimated from the type II frequency drift.
τ: duration of the solar event, estimated from the X-ray flux.
V_{SW}: speed of the solar wind at L1 at the time of the solar event.
Flare classification: classifications of the associated X-ray and optical flares, when available.

TABLE III
Observed and predicted arrival times for the 28 events in Table II.

Event number	SSC or SA date	SSC or SA time (UT)	TT_{obs} (hours)	TT_{stoa} (hours)	TT_{ispm} (hours)	TT_{spm} (hours)
1	790106	0127	51.65	62.8	49.0	58.1
2	790218	2027	66.63	68.0	68.8	58.0
3	790505	0850	63.83	81.9	mhd	66.6
4*	790705	0608	27.82	31.7	23.7	53.8
5	790706	1930	48.17	49.4	37.9	62.5
6	791107	1349	32.55	60.3	38.0	57.4
7	791111	0225	73.12	65.3	mhd	54.0
8	791222	0500	54.80	49.4	47.3	59.2
9	800411	1500	40.38	62.6	mhd	49.3
10	800524	0700	58.05	69.3	53.8	60.0
11	800606	1100	61.45	78.3	62.4	67.2
12	800825	2300	89.45	69.8	mhd	62.6
13	810219	1900	95.98	84.4	mhd	73.1
14	810301	0738	59.75	82.3	74.8	69.8
15	810407	1954	86.77	mhd	mhd	68.2
16	810412	1419	51.15	52.1	45.9	49.5
17	810411	1339	20.83	32.4	18.7	43.9
18	810426	0813	42.30	47.2	35.0	40.0
19	810514	1857	38.87	44.7	44.3	41.9
20	810517	2300	38.60	38.8	26.3	43.9
21	810830	2221	66.57	72.7	55.5	64.2
22	820606	1631	76.78	54.7	mhd	48.1
23	820609	0040	56.10	48.1	43.0	37.8
24	820619	0700	87.80	58.1	27.6	53.7
25	820622	1336	87.83	65.2	62.5	59.0
26	820624	1900	119.03	96.4	121.9	90.1
27	820724	1500	45.67	45.2	56.8	44.1
28	891020	0916	20.45	22.2	20.3	45.8

The parameters except for TT_{spm} are taken from Smith and Dryer (1995).
SSC: Geomagnetic Storm Sudden Commencement.
SA: shock observed by ISEE3, but no SSC.
This event is marked by asterisk after its event number.
TT_{obs}: observed transit time.
TT_{stoa}: transit time predicted by STOA.
TT_{ispm}: transit time predicted by ISPM.
TT_{spm}: transit time predicted by SPM.
mhd: The model (STOA or ISPM) predicts that this shock has decayed to an MHD wave before its arrival at L1.

TABLE IV

137 events during the period February 1997 to August 2002 and the predicted arrival times by our SPM model.

Event number	Begin date	Begin time (UT)	Shock arrival date	Shock arrival time (UT)	TT_{obs} (hours)	TT_{spm} (hours)
29	970207	0230	970209	1249	58.32	68.3
30	970407	1358	970410	1258	71.00	66.1
31	970512	0516	970515	0115	67.98	63.8
32	971104	0608	971106	2218	64.17	59.1
33	971127	1317	971130	0714	65.95	78.0
34	980126	2214	980128	1555	41.68	65.6
35	980519	0953	980523	0100	87.12	60.9
36	980611	1006	980613	1854	56.80	64.4
37	980808	0318	980811	2240	91.37	73.3
38	980824	2200	980826	0639	32.65	52.4
39	980903	1417	980906	0815	65.97	56.9
40	980923	0656	980924	2320	40.40	46.1
41	980930	1332	981002	0705	41.55	54.5
42	981020	2320	981023	1256	61.60	46.2
43	981105	1951	981108	0420	56.48	61.6
44	981128	0554	981130	0510	47.27	62.0
45	981223	0659	981226	0952	74.88	68.4
46	990120	2004	990122	1947	47.72	58.6
47	990209	0519	990211	0858	51.65	77.0
48	990216	0257	990218	0208	47.18	54.5
49	990216	2126	990221	2200	120.57	73.8
50	990308	0638	990310	0038	42.00	65.6
51	990622	1824	990626	0217	79.88	64.5
52	990629	0515	990702	0025	67.17	65.4
53	990711	0013	990713	0845	56.53	96.9
54	990719	0216	990722	0950	79.57	85.2
55	990725	1338	990728	1338	72.00	52.8
56	990728	1820	990730	1020	40.00	76.0
57	990801	2110	990804	0115	52.08	66.6
58	990806	1641	990808	1745	49.07	57.4
59	990820	2317	990823	1130	60.22	64.6
60	990821	1652	990823	1503	46.18	84.3
61	990828	1807	990831	0131	55.40	53.5
62	990830	1803	990902	0935	63.53	53.6
63	990913	1622	990915	2005	51.72	68.0
64	991117	0959	991119	2224	60.42	65.6

(Continued on next page)

TABLE IV
(Continued)

Event number	Begin date	Begin time (UT)	Shock arrival date	Shock arrival time (UT)	TT_{obs} (hours)	TT_{spm} (hours)
65	991120	2239	991123	1845	68.10	66.2
66	991124	2333	991128	1801	90.47	78.4
67	991222	0201	991226	2126	115.42	94.4
68	991228	0056	991230	1601	63.08	74.4
69	000118	1719	000122	0023	79.07	95.0
70	000208	0857	000211	0213	65.27	59.8
71	000210	0148	000211	2318	45.50	52.4
72	000212	0406	000214	0656	50.83	57.5
73	000218	0920	000220	2050	59.50	41.7
74	000404	1525	000406	1603	48.63	48.5
75	000420	2113	000424	0851	83.63	68.1
76	000430	0805	000502	1044	50.65	64.4
77	000510	1938	000512	1712	45.57	73.5
78	000512	2316	000516	1330	86.23	74.3
79	000520	0556	000523	2315	89.32	75.2
80	000606	1523	000608	0840	41.28	49.3
81	000607	1550	000611	0716	87.43	54.0
82	000615	1946	000618	1702	69.27	44.4
83	000618	0158	000621	1500	85.03	77.7
84	000620	1932	000623	1226	64.90	68.8
85	000707	1114	000710	0558	66.73	63.9
86	000710	2123	000713	0918	59.92	47.7
87	000712	2014	000714	1532	43.30	55.5
88	000714	1020	000715	1437	28.28	59.9
89	000717	2021	000719	1448	42.45	72.1
90	000722	1125	000725	1322	73.95	57.8
91	000725	0249	000728	0541	74.87	73.1
92	000901	1827	000906	1612	117.75	79.5
93	000912	1207	000915	0359	63.87	58.8
94	001001	1312	001003	0007	34.92	56.6
95	001009	2338	001012	2144	70.10	65.1
96	001029	0148	001031	1630	62.70	56.7
97	001101	1610	001104	0130	57.33	73.9
98	001108	2243	001110	0601	31.30	41.5
99	001123	2326	001126	0455	53.48	67.8
100	001125	1844	001128	0500	58.27	60.1

(Continued on next page)

TABLE IV
(Continued)

Event number	Begin date	Begin time (UT)	Shock arrival date	Shock arrival time (UT)	TT_{obs} (hours)	TT_{spm} (hours)
101	001126	0308	001129	0300	71.87	51.3
102	001126	1655	001129	0300	58.08	46.4
103	001129	0629	001203	0523	94.90	76.5
104	001218	1111	001221	1009	70.97	81.9
105	010110	0042	010113	0140	72.97	61.8
106	010120	2114	010123	1008	60.90	67.0
107	010128	1600	010131	0730	63.50	60.2
108	010211	0104	010212	2045	43.68	67.3
109	010215	1308	010220	0054	107.77	50.1
110	010315	2159	010319	1020	84.35	85.2
111	010318	0852	010322	1242	99.83	111.2
112	010324	0139	010327	0110	71.52	47.2
113	010328	1240	010330	2150	57.17	41.9
114	010329	1004	010331	0030	38.43	37.7
115	010331	1132	010402	2351	60.32	41.6
116	010402	2152	010404	1420	40.47	35.9
117	010405	1725	010407	1659	47.57	46.2
118	010406	1921	010408	1035	39.23	42.1
119	010409	1527	010411	1311	45.73	48.6
120	010410	0513	010411	1520	34.12	36.0
121	010411	1317	010413	0705	41.80	35.5
122	010415	1347	010418	0005	58.30	41.6
123	010418	0217	010421	1500	84.72	36.6
124	010426	1335	010428	0430	38.92	53.8
125	010524	1940	010527	1417	66.62	56.1
126	010615	1007	010618	0154	63.78	66.1
127	010730	2045	010803	0620	81.58	75.6
128	010814	1242	010817	1017	69.58	57.3
129	010825	1632	010827	1919	50.78	54.9
130	010828	1603	010830	1326	45.38	50.3
131	010830	0147	010901	0046	46.98	70.4
132	010830	2035	010901	0108	28.55	57.5
133	010909	1517	010914	0119	106.03	84.0
134	010925	0440	010929	0903	100.38	111.0
135	011009	1055	011011	1620	53.42	61.7
136	011019	0101	011021	1612	63.18	72.2

(Continued on next page)

TABLE IV

(Continued)

Event number	Begin date	Begin time (UT)	Shock arrival date	Shock arrival time (UT)	TT_{obs} (hours)	TT_{spm} (hours)
137	011025	1456	011028	0240	59.73	51.6
138	011104	1610	011106	0120	33.17	62.7
139	011108	0703	011109	0403	21.00	57.5
140	011117	0450	011119	1735	60.75	68.2
141	011121	1324	011124	0545	64.35	68.2
142	011122	2027	011124	0800	35.55	58.3
143	011122	2231	011124	0900	34.48	54.1
144	011226	0502	011229	0456	71.90	52.3
145	011228	2005	011230	1932	47.45	56.2
146	020103	0221	020107	1126	105.08	86.8
147	020123	1341	020126	1535	73.90	82.2
148	020127	1214	020131	2040	104.43	78.7
149	020224	1453	020228	0400	85.12	78.2
150	020312	2319	020315	1801	66.70	56.0
151	020315	2216	020318	1233	62.28	86.9
152	020318	0231	020320	1307	58.60	50.1
153	020414	0744	020417	1020	74.60	74.4
154	020417	0808	020419	0810	48.03	67.8
155	020421	0125	020423	0410	50.75	40.2
156	020507	0353	020510	1030	78.62	52.9
157	020516	0028	020518	1919	66.85	79.7
158	020517	0810	020521	2059	108.82	85.6
159	020521	2128	020523	1017	36.82	68.1
160	020715	2008	020717	1529	43.35	61.2
161	020717	0706	020719	0940	50.57	53.6
162	020718	0747	020719	1442	30.92	56.6
163	020723	0029	020725	1259	60.50	42.5
164	020726	2112	020729	1245	63.55	49.8
165	020729	0240	020801	0425	73.75	71.4

These events are taken from Fry *et al.* (2003) and McKenna-Lawlor *et al.* (2006). The events without corresponding IP shock arrival at 1 AU and those with ambiguous relationship between the solar event and the shock at 1 AU are not included here. The detailed input parameters for these events can be found in Fry *et al.* (2003) and McKenna-Lawlor *et al.* (2006). Begin time, TT_{obs}, and TT_{spm} are defined to be the same as in Table II and Table III. Shock Arrival time: year, month, day (YYMMDD), and time in UT of the arrival of the shock at near Earth spacecraft (such as ACE, WIND and SOHO) or the onset of SSC. Detailed information about these events can be found in Fry *et al.* (2003) and McKenna-Lawlor *et al.* (2006).

References

Arge, C. N. and Pizzo, V. J.: 2000, *J. Geophys. Res.* **105**, 10465.

Cho, K.-S., Moon, Y.-J., Dryer, M., Fry, C. D., Park, Y.-D., and Kim, K.-S.: 2003, *J. Geophys. Res.* **108**, 1445.

Dryer, M.: 1974, *Space Sci. Rev.* **15**, 403.

Dryer, M.: 1994, *Space Sci. Rev.* **67**, 363.

Dryer, M. and Smart D. F.: 1984, *Adv. Space Res.* **4**, 291.

Fry, C.D., Sun, W., Deehr., C. S., Dryer, M., Smith, Z., Akasofu, S. I., Tokumaru, M., and Kojima, M.: 2001, *J. Geophys. Res.* **106**, 20985.

Fry, C.D., Dryer, M., Smith, Z., Sun, W., Deehr, C.S., and Akasofu, S.-I.: 2003, *J. Geophys. Res.* **108**, 1070.

Fry, C. D., Dryer, M., Sun, W., Detman, T. R., Smith, Z., Deehr, C. S., Wu, C.-C., Akasofu, S.-I., and Berdichevsky, D.: 2004, *IEEE Trans. Plasma Sci.* **32**, 1489.

Gopalswamy, N., Lara, A., Lepping, R. P., Kaiser, M. L., Berdichevsky, D., and St. Cyr, O. C.: 2000, *Geophys. Res. Lett.* **27**, 145.

Gopalswamy, N., Lara, A., Yashiro, S., Kaiser, M. L., and Howard, R. A.: 2001, *J. Geophys. Res.* **106**, 29207.

Gopalswamy, N., Lara, A., Manoharan, P. K., and Howard, R. A.: 2005, *Adv. Space Res.* **36**, 2289.

Heinemann, M.: 2002, *J. Atmos. Terr. Phys.* **64**, 315.

Lewis, D. and Dryer, M.: 1987, NOAA/SEL Contract Report. to U.S. Air Weather Service.

Manoharan, P. K., Gopalswamy, N., Yashiro, S., Lara, A., Michalek, G., and Howard, R. A.: 2004, *J. Geophys. Res.* **109**, A06109.

McKenna-Lawlor, S. M. P., Dryer, M., Smith, Z., Kecskemety, K., Fry, C. D., Sun, W., Deehr, C. S., Berdichevsky, D., Kudela, K., and Zastenker, G.: 2002, *Ann. Geophys.* **20**, 917.

McKenna-Lawlor, S. M. P., Dryer, M., Kartalev, M. D., Smith, Z., Fry, C. D., Sun, W., Deehr, C. S., Kecskemety, K., and Kudela, K.: 2006, *J. Geophys. Res.* (submitted).

Moon, Y.-J., Dryer, M., Smith, Z., Park, Y.-D., and Cho, K.-S.: 2002, *Geophys. Res. Lett.* **29**, 1390.

Schwenn, R., Dal Lago, A., Huttunen, E., and Gonzalez, W. D.: 2005, *Annales Geophysicae* **23**, 1033.

Smart, D. F. and Shea, M. A.: 1985, *J. Geophys. Res.* **90**, 183.

Smart, D. F., Shea, M. A., Barron, W. R., and Dryer, M.: 1984, in M. A. Shea, D. F. Smart, and S. M. P. McKenna-Lawlor (eds.), *Proceedings of STIP Workshop on Solar/Interplanetary Intervals,* Bookcrafters Inc., Chelsea, MI., p. 139.

Smart, D. F., Shea, M. A., Dryer, M., Quintana, A., Gentile, L. C., and Bathhurst, A. A.: 1986, in P. Simon, G. R. Heckman, and M. A. Shea (eds.), *Proceedings of the Symposium on Solar-Terrestrial Predictions*, U.S. Govt. Print. Office, Washington, D C, p. 471.

Smith, Z. and Dryer, M.: 1990, *Solar Phys.* **129**, 387.

Smith, Z. and Dryer, M.: 1995, *NOAA Tech. Memo.* ERL/SEL-89.

Wei, F. S.: 1982, *Chinese J. Space Sci.* **2**, 63.

Wei, F. S. and Cai, H. C.: 1990, *Chinese J. Space Sci.* **10**, 35.

Wei, F. S., Cai, H. C., and Feng, X. S.: 2003, *Adv. Space Res.* **31**, 1069.

Wei, F. S. and Dryer, M.: 1991, *Solar Phys.* **132**, 373.

Wei, F. S., Feng, X. S., Xu, Y., and Fan, Q. L.: 2005, *Adv. Space Res.* **36**, 2363.

Wei, F. S., Xu, Y., and Feng, X. S.: 2002, *Sci. China (E)* **45**, 525.

Wei, F. S., Yang, G., and Zhang, G.: 1983, in Chen Biao and C. de Jager (eds.), *Proceedings of Kunming Workshop on Solar Physics and Interplanetary Travelling Phenomena*, Science Press, Beijing, Vol.2, p.1043.